Dynamic analysis of dislocation cores in the α-Fe lattice using the embedded atom model

K. D. Njoroge[1, 2, 5], G. O. Rading[1, 5], J. M. Kihiu [2, 5], M. J. Witcomb[3, 5], L. A. Cornish[3, 4, 5]

[1] Department of Mechanical and Manufacturing Engineering, School of Engineering, University of Nairobi, P.O. Box 30197-00100, Nairobi, Kenya.

[2] Department of Mechanical Engineering, School of Mechanical, Manufacturing and Materials Engineering, Jomo Kenyatta University of Agriculture and Technology, P.O. Box 62000-00200, Nairobi, Kenya.

[3] DST/NRF Centre of Excellence in Strong Materials, University of the Witwatersrand Private Bag 3, WITS, 2050, Johannesburg, South Africa.

[4] School of Chemical and Metallurgical Engineering, University of the Witwatersrand Private Bag 3, WITS, 2050, Johannesburg, South Africa.

[5] African Materials Science and Engineering Network (AMSEN)

Research done at the Department of Mechanical and Manufacturing Engineering, School of Engineering, University of Nairobi, P.O. Box 30197-00100, Nairobi, Kenya.

Abstract

The Embedded Atom Method (EAM) was employed to study the structure of body centered cubic (BCC) dislocation cores. Core energies, number of nearest neighbour atoms, stress tensor components, resolved shear stresses and dynamic dislocation core stresses were calculated for four types of dislocation cores. A dynamic dislocation model was presented and a "path of least resistance" (POLR) mechanism suggested for the determination of the Peierls stress. It was concluded that a sequence of stress components acting on the dislocation core in a $\{110\}\langle 111\rangle$ slip system were responsible for the proposed core atom motion resulting in the overall dislocation motion. A review of the resolved shear stress in the lattice was then used to collaborate the results of the dynamic dislocation model and the core atom motion mechanism model.

Key words: Embedded Atom Method, Dislocation, Peierls Stress, Body Centered Cubic

1. Introduction

The characterization of dislocation properties will frequently go beyond the simple continuum model and involve the lattice structure at the dislocation's core. The effects of the dislocation core have been found to be significant in the low temperature behavior of body centered cubic (BCC) metals [1], the plastic anisotropic behavior of ionic crystals [2, 3] and hexagonal close packed (HCP) metals [4], and the dislocation climb behavior in oxide crystals [5].

The Peierls-Nabarro model was the first successful model to account for the structure at the core of the dislocation [6]. A more accurate representation of the core configuration was later accomplished through lattice static or atomic models. Lattice static models are limited to the harmonic approximation, which is not strictly valid in the dislocation's core region. Atomic models are more suited to dealing with highly distorted lattice configurations [7]. In atomic models, the volume surrounding the core of the dislocation (region I) has been modeled as consisting of atoms interacting via a given non-linear potential, while the volume surrounding region I (region II) has been treated using the theory of elasticity. The power of the atomic models lies in their ability to accurately describe the core, which is dependent on the physical validity of the potentials used to describe the interaction among the atoms. A rigorous determination of the minimum energy with respect to the configuration of the dislocation core requires the use of quantum mechanical (QM) models. However, the highly distorted nature of the core severely limits the detail to which these interactions can be evaluated. The aim has been to find tractable approximate treatments, which are physically accurate over the range of distortions anticipated. The description of the core may then be used to predict the physical behavior of the dislocation in terms of its evolution and motion, and to determine the strain energy and the Peierls stress at which these physical actions take place.

The EAM has matured as a technique and is now applied in the study of material structures containing defects [8, 9, 10, 11]. Applications have been developed for the study of the structure of tilt boundaries [12, 13], phonon dispersion [14, 15], linear thermal expansion [15], point defects [14, 16, 17], and lattice dynamics [14, 18]. More recent research has focused on the modeling of potentials for application to industry specific problems. Potentials for studies on the effect of phosphorous on the embrittlement of nuclear reactor pressure vessels [19], the study of reactor pressure vessel steel thermal annealing [20], the generation of phase diagrams [1, 21], and the dissolution and diffusion of hydrogen in bulk α-Fe as well as binding of hydrogen to surfaces, vacancies and dislocations [22] are available. However, the simulation of the dynamic-spatial atomic

structure of dislocation cores, and its contribution to the behavior of dislocations viewed as an atomic scale problem, has not been comprehensively addressed. There exists opportunity to advance the development and application of potentials to model dislocation cores and dislocation families for the application to a wider range of industrial problems.

2. Method

This work generated the dislocated structure by the application of a set of displacement vectors to the points of a perfect lattice about a prescribed dislocation core centre. The dislocation line direction was set as $\frac{1}{2}[1\bar{1}1]$. The distortion was introduced and the slip plane created by displacing the block of atoms on one side of a predetermined plane by half a Burgers vector. A transition zone was formed around the dislocation core where the first and second rows of atoms were displaced at 1/6 and 1/3 of the Burgers vector.

The direction of the Burgers vector was defined for the pure edge, pure screw and mixed dislocations as that direction, oriented such that together with the dislocation line vector, defined the dislocation type, and such that this direction resulted in a whole number of lattice displacements for the defined dislocation type. Consequently, two pure and two mixed dislocations were possible for the body centred cubic (BCC) lattice. These were the pure screw, the 35.26 degree screw, the 70.53 degree screw and the pure edge dislocations. The dislocation core was formed at the intersection of the slipped and un-slipped block of atoms at the edge of the slip plane. The use of the different displacement vectors resulted in the generation of the different types of dislocation cores.

Simulation was carried out for static and dynamic conditions. The dynamic conditions were generated by moving the block of atoms on one side of the slip plane by predefined displacement vectors. These displacement vectors were set to a fraction of the Burgers vector for each dislocation type, within the slip plane.

This work applied the Embedded Atom Method (EAM) potential of Mendelev et al. [23] to evaluate the cohesive strength and stress tensor of the four different types of dislocation cores. This potential has been tested and found to stabilize the non-degenerate dislocation cores on $\{110\}$ glide planes in agreement with experimental data for dislocation motion at low temperatures [24]. The cohesive strength and the stress tensors for the dynamic simulations were calculated after each incremental displacement giving rise to a varying strength and stress profile.

Code was prepared on a Fortran 90 platform and the computation utilized a single scale atomic model with an extended "region I" of 1331 atoms in an "11 x 11 x 11" block of atoms to carry out the simulations. This was in variation to the traditional atomic model [7], as it eliminated the need to couple the two windows of resolution.

This paper presents results on the simulation of the behavior of the dislocation cores. Section 1 presents results from the review of the cohesive strength and stress tensor of the dislocation core at equilibrium lattice spacing. This is followed by Section 2, which presents a dynamic dislocation stress analysis.

3. Results And Discussions

3.1. Static Analysis

The cohesive strengths of the static dislocated lattices are given in Table 1. These results were obtained from simulations for the four types of dislocation cores and compared with the results for the perfect lattice. The results revealed a reduction of cohesive strength with the introduction of dislocations, consistent with empirical observations. However, the differences in cohesive strength were small (less than 1%), hence the results were only of qualitative value. Whereas the pure screw dislocation presented a higher cohesive strength per atom than the edge dislocation, indicating higher edge dislocation mobility consistent with empirical findings [25, 26], the 70.53 degree screw did not show a high cohesive strength, which was inconsistent with empirical findings, which report that the 70.53 degree mixed dislocation has exceptionally high Peierls stress [27].

Two reasons were suggested for these observations. The first was that these results were generated from simulations of a static lattice structure, providing a snapshot of the comparative cohesive strength of the equilibrium lattice. This state may not be that where the Peierls stress would be determined. The second was that the lack of gradient terms in the formulation of the cohesive strength may render the computation incapable of capturing the distortion gradient in the dislocation core. This suggestion was reasonable as it is observed that the embedding energy did not vary with the type of dislocation, while the pairing energy varied only marginally. The evaluation of the dynamic dislocation was used to explore the first assertion, while the use of a gradient sensitive electron density function was suggested as a test of the second assertion.

The cohesive energy per atom about the dislocation core was taken as a measure of the limiting stress required to overcome inter atomic bonding, to enable dislocation glide. This was then related to the macroscopic yield stress by the amalgamation of the various effects of the density of dislocations contained in the matrix. However, the above results illustrated the shortcomings of this approach, and the postulated hypothesis that a gradient-based EAM functional was more suitable, will be evaluated elsewhere. The use of dislocation dynamics for the direct computation of the Peierls stress was feasible and its

application has been supported by existing literature where empirical findings relate the macroscopic yield stress to the Peierls stress at low temperatures [28].

Table 1: Embedding and pair energy contributions to the cohesive energy for four types of dislocations (eV/atom).

Dislocation type	Embedding energy, F(ρ)	1st Pair potential, $V(r_{ij})$	2nd Pair potential, $V(r_{ij})$	3rd Pair potential, $V(r_{ij})$	Cohesive energy / atom, E_c (eV)	No. of nearest neighbours	Burgers vector direction
Pure screw	-5.495193	1.48466	0	0	-4.01053	57	$[\bar{1}\,1\,\bar{1}]$
70.53^O screw	-5.495193	1.48539	0	0	-4.009801	57	$[\bar{1}\,1\,0]$
35.26^O screw	-5.495193	1.48466	0	0	-4.01053	57	$[\bar{1}\,1\,1]$
Pure edge	-5.495193	1.48514	0	0	-4.010046	56	$[\bar{1}\,1\,2]$
Perfect lattice	-5.495382	1.48328	0	0	-4.012102	58	-

Simulations were also carried out to generate the stress tensor components at the dislocation core. These values represented the resulting stress due to lattice distortion forming the dislocation core. Six stress tensor components were generated with the remaining three obtained by application of principle of complimentary stress.

Table 2: Stress tensor components calculated for four types of dislocations (GPa.).

Dislocation type	σ_{11}	σ_{12}	σ_{13}	σ_{22}	σ_{23}	σ_{33}
Pure screw	1.4817	-6.2778	-5.1545	4.1319	-5.6076	3.7813
70.53 degree screw	-2.163	-7.6378	-5.5587	4.6258	-5.7451	2.6820
35.26 degree screw	1.4947	-6.2258	-5.1025	4.3527	-5.4128	4.0021
Pure edge	2.2437	-7.1664	-5.0673	1.9309	-5.8403	3.7959

Results presented in Table 2 revealed that the lowest stresses were the σ_{11} tensor component, which corresponded to $[100]$ direction, and the σ_{22} tensor component, which corresponded to the $[010]$ direction. The $\langle 100 \rangle$ directions were of interest as dislocations in these directions contribute substantially to the flow stress [29] and are formed by the interaction of two $\frac{1}{2}\langle 111 \rangle$ dislocations. The resulting stress components suggested that two or more stress components combined to generate the $\langle 110 \rangle$ type motion. Additionally, dislocation core reconstruction across a $\langle 110 \rangle$ zone axis was attributed to the similar combination of stress components. This was consistent to observations of dissociation of screw dislocation cores across adjacent (110) planes [30, 31, 32]. The intersection of non-coplanar dislocations and their interaction was enhanced by the presence of a $\langle 110 \rangle$ zone axis. In addition, edge dislocation core spreading to adjacent (112) planes has been reported [33]. It was proposed that dislocation core spreading and core-core interaction be explained by the analysis of combination of dislocation core stress components.

The precise motion of the individual atoms was not determined, but the values of the stress tensor components suggested that motion in the $[100]$, $[010]$ and $[001]$ directions was to be expected. This motion corresponded to atomic movement in different $\{110\}$ and $\{112\}$ planes belonging to the given $\langle 110 \rangle$ zone axis. The very nature of a 3-dimensional lattice suggested that out-of-plane motion was necessary for the "micro-cleavage" of the lattice to enable dislocation motion. Additionally, the presence of the $\langle 110 \rangle$ zone axis enabled the out-of-plane motion to occur at the lower stress levels

corresponding to the [100], [010] and [001] directions. This visualization for dislocation core evolution was consistent with observations of moderate non-planar spreading of dislocation cores in BCC lattice [32].

3.2. Dynamic Analysis

Peierls stress calculations have concentrated on the body centered cubic (BCC) metals because it was realized that their dislocation core effects contribute to a high Peierls stresses. Dislocation dissociation in BCC metals is localized to the core region (there is no stable stacking fault separating the partials) and, in the case of the ⟨111⟩ screw dislocation, it is non-planar. The BCC screw dislocation core is rather compact and this gives rise to a large Peierls stress [34].

Figures 1 to 5 present the variation of the lattice stress about the dislocation core as the dislocation moves rigidly along the direction of its Burger's vector. All the dislocations presented different sinusoidal stress component variation. These curves suggested that the movement of atom rows past rows of other atoms was synchronised, enabling the simulation to detect the variation. The positive and negative values were interpreted as tensile and compressive stresses respectively and it was noted that the direct stresses were positive (except for σ_{11} component where the troughs dip below zero) and the shear stresses are negative. It was expected that movement of atoms around the dislocation core resulting in dislocation motion would follow the path of least resistance (POLR) and would involve changes in direction.

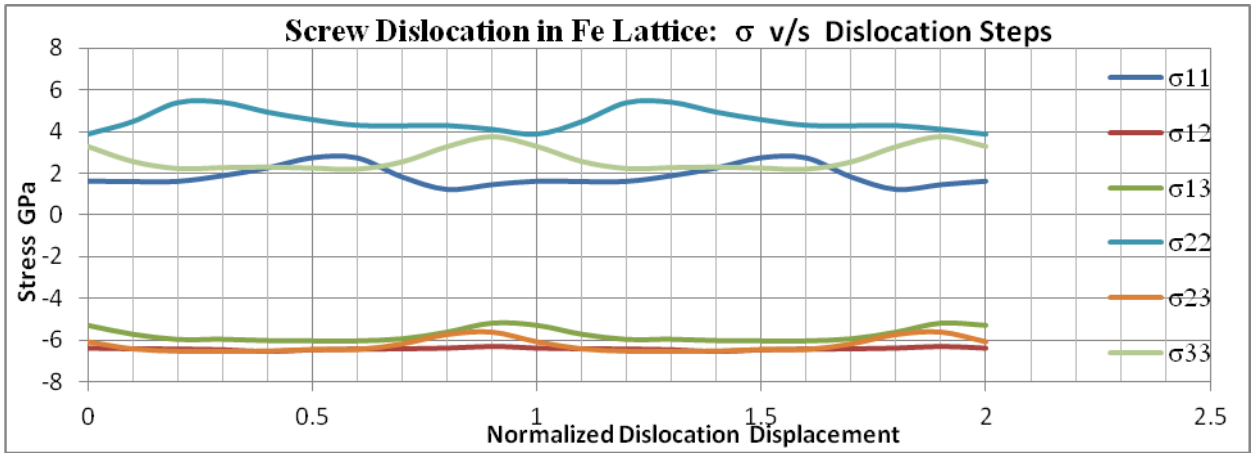

Fig 1: Variation of the stress generated as a pure screw dislocation in Fe lattice moves in the $[1\bar{1}1]$ direction.

The stress cycle for the pure screw is presented in Figure 1. The POLR was in the σ_{11} direction over most of the path. At some point, the curve for σ_{11} intersected that of σ_{33} and exceeded it for a short potion of the cycle. Over this period, σ_{33} was at its lowest value and provided the POLR, after which σ_{11} resumed as the POLR. This sinusoidal path oscillated between 1.26GPa and 2.27GPa. This compared well with published values of the Peierls stress of 1.2 to 1.8GPa from Chaussidon et al. [24] and 1.3 to 1.9GPa from Ventelon [35] for BCC Fe. The stress component σ_{11} corresponded to motion along the (011) plane, and involved displacement of atoms away from the (110) glide plane ahead of the dislocation core. The stress component σ_{33} corresponded to motion along the (110) plane, and involved displacement of atoms along the glide plane ahead of the dislocation core. The proposed sequence supported the hypothesis that dislocation motion occured predominantly by the "peeling" of atoms around the dislocation core as a stress-enabled mechanism. The shear stresses were in the order of magnitude -6.44GPa, with smaller amplitude than the direct stresses. Additionally, the magnitude of the shear stresses was of the same order of magnitude as the peak direct stresses of 5.41GPa. These higher stress values were an indication of the stress required to generate catastrophic fracture of the lattice. Consequently, it was reasonable to infer that the ultimate tensile stress should be in the order of 2.8 times the yield stress. This result was obtained by comparing the maximum stress values related to catastrophic failure and those related to dislocation motion and hence material yielding.

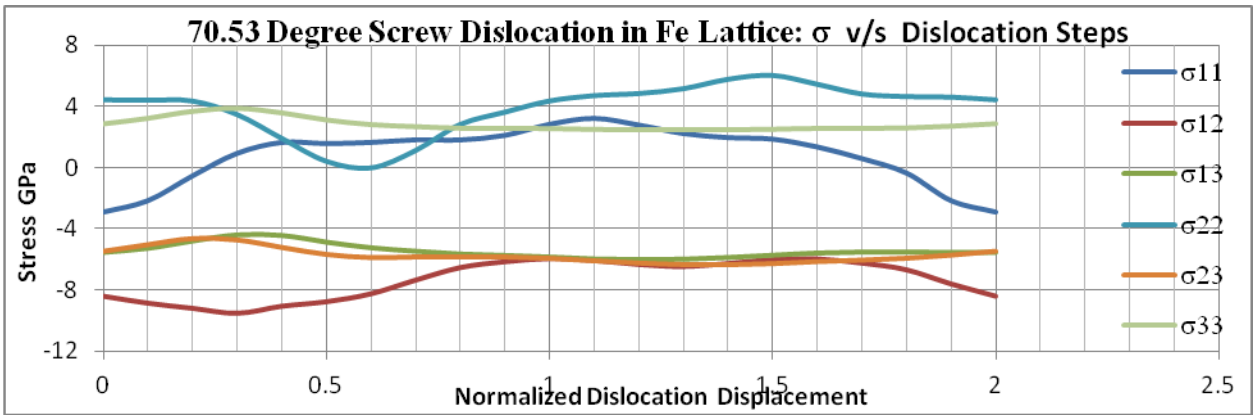

Fig 2: Variation of the stress generated as a 70.53 degree screw dislocation in Fe lattice moves in the $[\bar{1}10]$ direction.

The stress component cycles for the 70.53 degree screw are presented in Figure 2. The POLR was along the direction corresponding to the σ_{11} stress component. It was noteworthy that this stress component traversed the zero stress value, with a maximum positive value 3.21GPa and a maximum negative value of -2.91GPa. This curve intersected that of σ_{22} at 1.91GPa and σ_{33} at 2.54GPa at different periods of the cycle. The intersection occurred over a small interval, and the resulting change in POLR, for the atoms around the dislocation core traversed three directions. The larger maximum value of σ_{11} (though negative in sign) implied that a 70.53 degree screw was harder to move than a pure screw dislocation. In comparison to the results for the pure screw dislocation, the maximum direct stress increased to 6.06GPa, with a corresponding increase of the maximum shear stress value to -9.55GPa. The larger value of the maximum shear stress and the divergence in shear stress curves implied that a narrow band catastrophic ultimate stress would not result from the presence of 70.53 degree screw dislocations. These results were supported by empirical findings [27] that report that an exceptionally high Peierls stress is experienced by the 70.53 degree screw.

The stress component curves for the 35.26 degree screw are presented in Figure 3. The POLR was again along the direction corresponding to the σ_{11} stress component. This stress component oscillated between a maximum value of 2.76GPa and a minimum value of 1.27GPa. The POLR changed direction when the σ_{22} stress component curve intersected with the σ_{11} stress component curve at about 2.42GPa. The σ_{22} stress component corresponded to motion on the (011) plane, and involved movement of atoms away from the slip plane around the dislocation core. A maximum magnitude shear stress of -6.51GPa was noted, with a spread of the shear stress components similar to that of the pure screw dislocation. This implied that a narrow band catastrophic ultimate stress may result from the 35.26 degree screw dislocation.

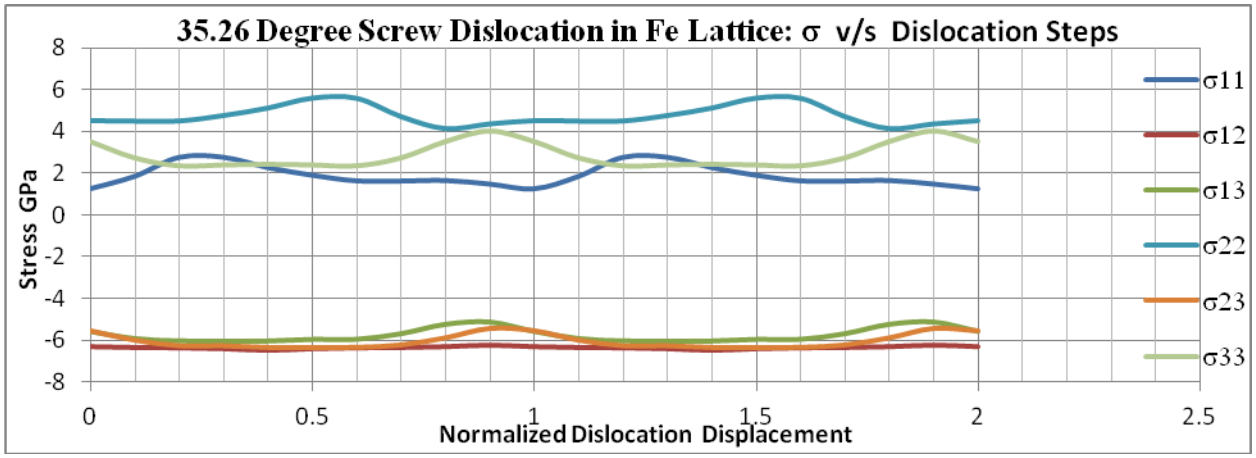

Fig 3: Variation of the stress generated as a 35.26 degree screw dislocation in Fe lattice moves in the $[\bar{1}11]$ direction.

Results on simulations for the pure edge dislocation presented in Figure 4 presented the most random curves for the four types of dislocations. Similar sinusoidal curves were obtained for the shear stress components. The POLR was again provided by the curve corresponding to the σ_{11} stress component, which spanned the range -0.848GPa to 2.45GPa. Along this curve, intersection with σ_{22} stress component curve at 1.93GPa and σ_{33} stress component curve at 2.4GPa occurred with corresponding change in direction into adjacent zone $\langle 110 \rangle$ axis planes. The availability of a larger number of atom motion directions, only replicated by the 70.53^{O} screw, was envisaged as the possible mechanism for a greater mobility of the dislocation core. Additionally, this dislocation presented the lowest magnitude stress of -0.848GPa, which was considered to enhance dislocation motion over other types of dislocations. The spreading of the shear stress curves suggested that a narrow band catastrophic ultimate stress would not result from these dislocations.

The curves in Figures 1 to 4 demonstrate that the Embedded Atom Method (EAM) formulation applied to evaluate the Peierls stress had the required sensitivity to differentiate between the dislocation types. This supported the earlier assertion that dislocation dynamics based upon the EAM model presented a more complete description in material defect analysis. Specifically, it was suggested that the interaction of combinations of stress components resulted in the POLR, and therefore determined the Peierls stress profile. The lack of symmetry of the stress curves resulted from the effects of the twinning/anti-twinning asymmetry of the BCC lattice, and this was therefore more pronounced for the edge dislocation. The short range nature of the EAM potential resulted in a stress computation at the dislocation core only. It was proposed that a more complete approach would be to generate stress components due to dislocation cores at locations removed from the dislocation core. This would be invaluable in the study of dislocation interaction with other dislocations, obstacles and grain boundaries. Thus, there was need for the development of a longer range potential, specifically suited to dislocation interaction.

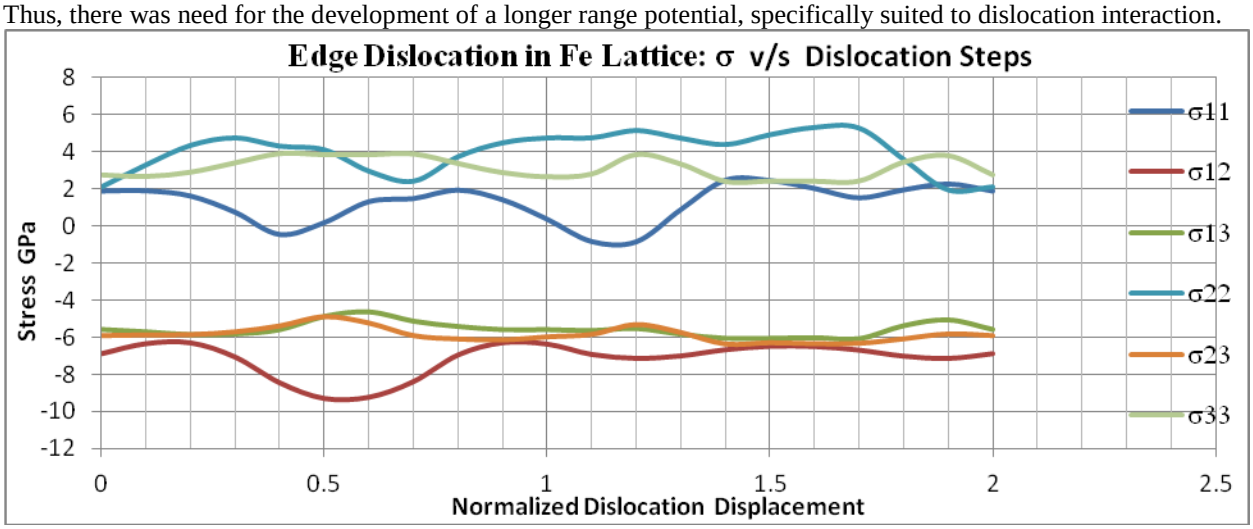

Fig 4: Variation of the stress generated as a pure edge dislocation in Fe lattice moves in the $[\bar{1}12]$ direction.

Schmid's law [36] states that glide on a given slip system is controlled by the resolved shear stress on that system known as the Schmid stress, and in a rate-independent formulation, glide commences when this stress reaches a critical value known as the critical resolved shear stress (CRSS). Implied is that plastic deformation should not be affected by non-glide stress tensor components and is largely dependent on the existence of planar dislocation dissociation mechanisms. For body centered cubic (BCC) lattice structures, stress tensor components in associated $\{110\}$ planes may act on dislocation cores spread into these associated planes resulting in non-glide stresses contributing to plastic deformation. Non-Schmid behaviour of BCC metals therefore results from the three way dislocation core dissociation or spreading on associated $\{110\}$ zone planes and is supported by atomistic calculations [26, 37, 38, 39]. However, a convergence of atomistic calculations and experimental results is lacking, with computations overestimating the Peierls stress [40, 41]. The resolved shear stress in the direction of the Burger's vectors is presented in Figure 5.

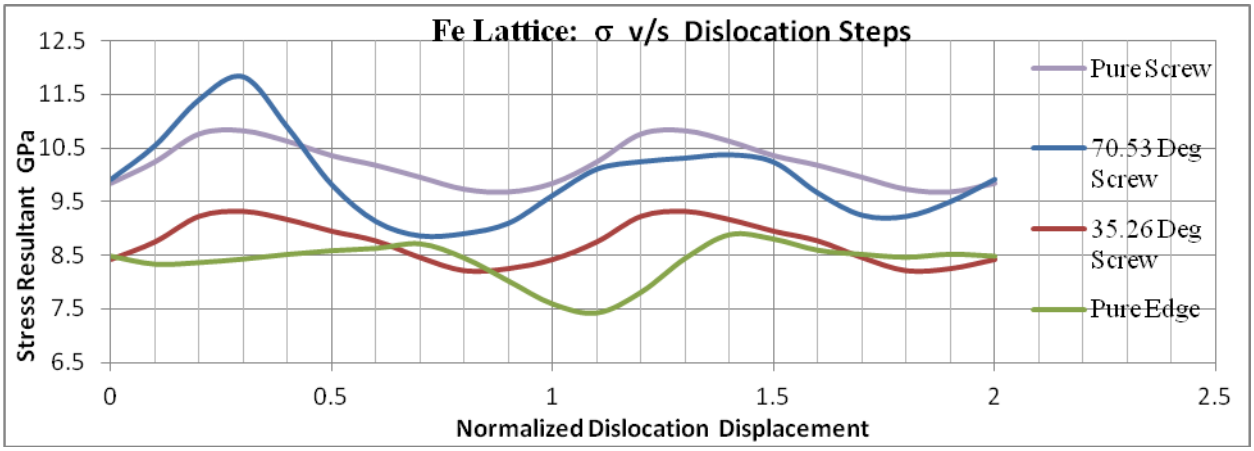

Fig 5: Variation of the resolved stress generated as a dislocation in Fe lattice moves in the direction of the burgers vector.

Figure 5 summarised the results of Figures 1 to 4 and revealed that the edge dislocation provided the least resolved shear stress over most of the dislocations motion. It was therefore inferred that the edge dislocation possessed the greatest mobility consistent with empirical findings [25]. The 70.53 degree screw dislocation presented a curve with a much higher amplitude and peak stress value. This was again consistent with empirical findings, which reported its high Peierls stress [27]. Also noteworthy was that the magnitude of the resolved shear stress was much higher than both experimental and calculated Peierls stress [35]. Therefore it is inferred that the Peierls stress was related to the active stress components, and not to the overall resolved shear stress.

4. Conclusions And Recommendations

The application of the Embedded Atom Method (EAM) to the evaluation of the cohesive strength and the stress tensor at the dislocation core, using a single static window of resolution, demonstrated the limitation of the technique and led to the proposal that dynamic dislocation analysis or a gradient-based functional be developed to enhance the method's sensitivity to distortions at the dislocation core. Stress components generated at equilibrium lattice conditions were used to show the potential relation between the evolution of the dislocation core and the specific displacements related to the stress components.

Analysis of the dislocation in motion was also presented and a "path of least resistance" POLR mechanism proposed to explain the evolution of the dislocation core. These results illustrated the contribution of different stress components to the motion of atoms about the core and supported the proposed "peeling" of atoms about the core. A comparison of the resolved shear stress in the lattice provided a alternative view to collaborate the results obtained from the analysis of the dynamic dislocation core and the proposed mechanism explaining the motion of the dislocation core atoms. Finally, it was concluded that the Peierls stress was related to the active stress components, and not to the overall resolved shear stress.

Acknowledgements

This research is funded by the African Material Science and Engineering Network (AMSEN) vote no. 500-661-382, a Carnegie-IAS Regional Initiative in Science and Education Network. This research is also supported by the Jomo Kenyatta University of Agriculture and Technology. This support is greatly appreciated.

References

1. **G. Bonny, R. C. Pasianot, L. Malerba,.** Fitting Interatomic Potentials Consistent with Thermodynamics: Fe, Cu, Ni and their Alloys. *Philosophical Magazine.* 2009, Vol. 89, 34-36, pp. 3451-3464.
2. **M. P. Puls.** Liblice : s.n., 1983. Proceedings of "The Structure and Properties of Crystal Defects".
3. **W. Skrotzki, P. Haasen.** Hardening Mechanisms of Ionic Crystals on {110} and {100} Slip Planes. *Journal Physical Science.* 1981, Vol. 42, C3, pp. 119-148.
4. **D. J. Bacon.** Liblice : s.n., 1983. Proceedings of "The Structure and Properties of Crystal Defects".
5. **T. Bretheau, J. Castaing, J. Rabier, P. Veyssiere.** Dislocation Motion and High Temperature Plasticity of Binary and Ternary Oxides. *Advances in Physics.* 1979, Vol. 28, 6, pp. 835-1014.
6. **F. R. N. Nabarro.** Dislocations in a Simple Cubic Lattice. *Proceedings of the Physical Society.* 1947, Vol. 59, 2, pp. 256-272.

7. **M. P. Puls.** *Dislocation Modeling of Physical Systems.* [ed.] R. Bullough, G.S. Hartley, J.P. Hirth, M.F. Ashby. New York : Pergamon Press, 1981. p. 249.
8. **M. S. Daw, M. I. Baskes.** Embedded Atom Method: Derivation and Applications to Impurities, Surfaces, and Other Defects in Metals. *Physical Review B.* 1984, Vol. 29, pp. 6443-6453.
9. **F. Ercolessi, M. Parrinello, E. Tosatti.** Simulation of Gold In The Glue Model. *Philosophical Magazine A.* 1988, Vol. 58, pp. 213-226.
10. **S. M. Foiles, M. I. Baskes, M. S. Daw.** Embedded Atom Method Functions for the FCC Metals Cu, Ag, Au, Ni, Pd, Pt and their Alloys. *Physical Review B.* 1986, Vol. 33, 12, pp. 7983-7991.
11. **M. S. Daw, S. M. Foiles, M. I. Baskes.** The Embedded-Atom Method: A Review of Theory and Applications. *Materials Science Reports.* 1993, Vol. 9, pp. 251-310.
12. **M. Yan, M. Sob, G. J. Ackland, D. E. Luzzi, V. Vitek, M. Methfessel, C. O. Rodriguez.** Interatomic Forces and Atomic Structure of Grain Boundaries in Copper-Bismuth Alloys. *Physical Review B.* 1993, Vol. 47, 10, pp. 5571-5583.
13. **R. Besson, A. Fraczkiewicz, M. Biscondi.** An Empirical Many-body Potential for B2 Fe Al. *Journal De Physique IV.* 1996, Vol. 6, C2, pp. 47-52.
14. **G. J. Ackland, D. J. Bacon, A. F. Calder, T. Harry.** Computer Simulation of Point Defect Properties in Dilute Fe-Cu Alloy using a Many-body Interatomic Potential. *Philosophical Magazine A.* 1997, Vol. 75, 3, pp. 713-732.
15. **W. Zang, Q. Xie, X. Ge.** Interatomic Potentials Between Distinct Atoms from First Principles Calculation and Lattice Inversion Method. *Journal of Applied Physics.* 1997, Vol. 82, 2, pp. 578-582.
16. **C. Domain, C. S. Becquart.** Ab Initio Calculations of Defects in Fe and Dilute Fe-Cu Alloys. *Physical Review B.* 2001, Vol. 65, 024103, pp. 1-14.
17. **T. T. Lau, C. J. Forst, X. Lin, J. D. Gale, S. Yip, K. J. V. Vliet.** Many-Body Potential for Point Defects Clusters in Fe-C Alloys. *Physical Review Letters.* 2007, Vol. 21, 5501, pp. 1-4.
18. **R. C. Pasianot, L. Malerba.** Interatomic Potentials Consistent with Thermodynamics: The Fe-Cu System. *Journal of Nuclear Materials.* 2007, Vol. 360, pp. 118-127.
19. **G. J. Ackland, M. I. Mendelev, D. J. Srolovitz, S. Han, A. V. Barashev.** Developement of Interatomic Potential for Phosphorous Impurities in alpha-Iron. *Journal of Physics: Condensed Matter.* 2004, Vol. 16, 27.
20. **G. Bonny, R. C. Pasianot, N. Castin, L. Malerba.** Ternary Fe-Cu-Ni Many-Body Potential to Model Reactor Pressure Vessel Steels: First Validation by Simulated Annealing. *Philosophical Magazine.* 2009, Vol. 89, 34-36, pp. 3531-3546.
21. **G. Bonny, R. C. Pasianot, L. Malerba.** Fe-Ni Many-Body Potential for Metallurgical Applications. *Modelling and Simmulation in Materials Science and Engineering.* 2009, Vol. 17, 025010, pp. 1-13.
22. **A. Ramasubramaniam, M. Itakura, E. A. Cater.** Interatomic Potentials for Hydrogen in Alpha-Iron based on Density Functional Theory. *Physical Review B.* 2009, Vol. 79, 174101, pp. 1-13.
23. **M. I. Mendelev, S. Han, D. J. Srolovitz, G. J. Ackland, D. Y. Sun, M. Asta.** Development of Interatomic Potentials appropriate for Crystalline and Liquid Iron. *Philosophical Magazine.* 2003, Vol. 83, 35, pp. 3977-3994.
24. **J. Chaussidon, M. Fivel, D. Rodney.** The Glide of Screw Dislocations in BCC Fe: Atomistic Static and Dynamic Simulations. *Acta Materialia.* 2006, Vol. 54, 13, pp. 3407-3416.
25. **T. Imura, K. Noda, H. Matsui, H. Saka, H. Kimura.** *Dislocations in Solids.* Tokyo : University of Tokyo Press, 1985. p. 287.
26. **M. S. Duesbery.** On Kinked Screw Dislocations in the BCC Lattice - I. The Structure and Peierls Stress of Isolated Kinks. *Acta Metallurgica.* 1983, Vol. 31, 10, p. 17471758.
27. **V. Vitek, M. Yamaguchi.** Core Structure of Non-screw 1/2[111] Dislocations on (110) Planes in B.C.C. Crystals, II. Peierls Stress and the Effect on an External Shear Stress on the Cores. *Journal of Physical F. Metal Phys.* 1973, Vol. 3, 3, pp. 537-542.
28. **M. Tang, L.P. Kubin, G.R. Canova.** Dislocation Mobility and the Mechanical Response of BCC Single Crystals: A Mesoscopic Approach. *Acta Materialia.* 1998, Vol. 46, pp. 3221-3235.
29. **W. Carrington, K. F. Hale, D. McLean.** Arrangement of Dislocations in Iron. *Proceedings of the Royal Society of London, Series A, Mathematical and Physical Sciences.* 1960, Vol. 259, 1297, pp. 203-227.
30. **A. H. Cottrell, B. A. Bilby.** A Mechanism for the Growth of Deformation Twins in Crystals. *Philosophical Magazine.* 1951, Vol. 42, 329, pp. 573–581.
31. **F. C. Frank, J. F. Nicholas.** Stable Dislocations in the Common Crystal Lattice. *Philosophical Magazine.* 1953, Vol. 44, 358, pp. 1213-1235.
32. **J. B. Cohen, R. Hinton, K. Lay, S. Sass.** Partial Dislocations on the {110} Planes in the BCC Lattice. *Acta Metallurgica.* 1962, Vol. 10, 9, pp. 894-895.

33. **D. A. Terentyev, Y. N. Osetsky, D. J. Bacon.** Effects of Temperature on Structure and Mobility of the <100> Edge Dislocation in Body Centered Cubic Iron. *Acta Materialia.* 2010, Vol. 58, pp. 2477-2482.
34. **V. Vitek.** Core Structure of Screw Dislocations in BCC Metals: Relation to Symmetry and Inter Atomic Bonding. *Philosophical Magazine.* 2004, Vol. 84, 3-5, pp. 415-428.
35. **L. Ventelon.** *Core Structure of Screw Dislocations in Fe From First-Principles.* Department of Materials for Nuclear Energy at the Nuclear Energy Division, Service de Recherches de Métallurgie Physique. Yvette, France : Commissariat à l'énergie Atomique et aux Energies Alternatives, 2008. PhD Thesis.
36. **J. P. Hirth, J. Lothe.** *Theory of Dislocations.* 2nd. s.l. : John Willey & Sons, 1982.
37. **J. Chang, W. Cai, V.V. Butalov, S. Yip.** Dislocation Motion in BCC Metals by Molecular Dynamics. *Materials Science and Engineering A.* 2001, Vols. 309-310, pp. 160-163.
38. **K. Edagawa, T. Suzuki, S. Takeuchi.** Motion of a Screw Dislocation in a 2 Dimensional Peierl's Potential. *Physical Review B.* 1997, Vol. 55, 10, pp. 6180-6189.
39. **W. Xu, J. Moriarty.** Accurate Atomistic Simmulations of the Peierl's Barrier and Kink-Pair Formation Energy for <111> Screw Dislocations in BCC Mo. *Computational Material Science.* 1998, Vol. 9, 3-4, pp. 348-356.
40. **H. J. Kaufmann, A. Luft, D. Schulze.** Deformation Mechanism and Dislocation Structure of High Purity Molybednum Single Crystals at Low Temperatures. *Crystal Research Technology.* 1984, Vol. 19, 3, pp. 357-372.
41. **S. Takeuchi, K. Maeda.** Slip in High Purity Tantalum between 0.7 and 40 K. *Acta Metallurgica.* 1977, Vol. 25, 12, pp. 1485-1490.